Int. J. Electrochem. Sci., 17 **(2022)** Article Number: 220764, doi: 10.20964/2022.07.68

International Journal of
ELECTROCHEMICAL
SCIENCE
www.electrochemsci.org

An Online Method for Power State Estimation of Lithium-Ion Batteries under the Constraints of the Fusion Model Considering Temperature Effect

Jian Wang[1], *Shunli Wang*[1,*], *Chunmei Yu*[1], *Bowen Li*[2], *Mingfang He*[1]

[1] School of Information Engineering, Southwest University of Science and Technology, Mianyang 621010, China;
[2] School of Pharmacy and Life Sciences, Robert Gordon University, Aberdeen, AB10-7GJ, UK
[*]E-mail: wangshunli@swust.edu.com

Received: 1 April 2022 / *Accepted:* 13 May 2022 / *Published:* 6 June 2022

As the main source of energy storage and power supply for new energy vehicles, the state of power of the power lithium-ion battery reflects the maximum power that the vehicle can provide. However, the ambient temperature of the automotive battery pack in the process of use is complex and variable. To address the challenge of achieving high accuracy in power estimation, an adaptive forgetting factor recursive least squares method based on improved bias compensation is proposed to achieve online tracking of state of power estimation with the fusion model limitation of voltage, current and charge state as influence factors and combined with parameter correction of temperature influence. The experiments show that the algorithm has a voltage error lower than 0.08V and an online power calculation error lower than 6W under BBDST conditions.

Keywords: state of power; power lithium-ion battery; adaptive forgetting factor recursive least squares method based on improved bias compensation; fusion model limitation of voltage, current and charge state; parameter correction of temperature influence

1. INTRODUCTION

Due to the advantages of high energy density, high energy efficiency ratio, clean and pollution-free, power lithium-ion batteries have become the core of the power system of new energy vehicles [1-4]. The accurate prediction of the state parameter characteristics of the power lithium-ion batteries can provide users with reliable data reference, which can be used not only to improve the product experience, but also to effectively ensure driving safety[5-7]. Nowadays, as the product price of power lithium-ion batteries decreases, more and more car manufacturers start to release new energy vehicle development plans [8, 9]. The application scenarios of new energy vehicles are changing every moment.

High range and high sustained power output and safety have constrained the development of new energy vehicles [10-13]. Battery management systems no longer rely solely on a single battery indicator (SOC, etc.) to provide information for users [14, 15]. The State of Power (SOP) of a power lithium-ion battery is defined as the maximum output power that the battery can provide in a continuous period, and it is usually strongly coupled with the voltage and circuitry of the battery [16, 17]. The SOP can effectively characterize the power output characteristics of the vehicle, and analyzing the power output characteristics which can help optimize the energy output of the vehicle and enhance the battery energy management, thus improving the experience of using the vehicle [18].

Closely related to the foregoing is the fact that the state parameter characterization of a powered lithium-ion battery is often reflected by the construction of models[19-21]. Ma, Yan et al. established a simplified first-order electrochemical-thermal coupling model to observe the internal parameters of the battery by optimizing the two-site model of the lithium-ion battery [22]. Li, Junfu analyzed the effects of the internal parameters of the higher coulomb efficiency battery (including solid-phase diffusion, liquid-phase diffusion and reaction polarization, etc.) and established an electrochemical model considering the effects of high coulomb efficiency[23]. Chen, Ning proposed to construct an equivalent circuit model of electrochemical impedance based on fractional-order theory and introduced the butler-volmer equation to address the effect of temperature to establish the model under wide excitation, which is superior to the pseudo-2-dimensional model under high-frequency excitation [24]. Zhang, Ji'ang et al. applied the electrochemical impedance spectrum theory and proposed a variable-order equivalent circuit model to achieve higher accuracy and adaptability[25]. However, the power lithium-ion batteries have a complex and variable use scenario in the whole vehicle application, and the ambient temperature has a strong inhibitory or activating effect on the electrochemical characteristics of the lithium-ion batteries. Considering the influence of temperature variation, the long test cycle for acquiring the parameters of the above model, the high complexity of calculation and the large error of interference of environmental variables are not conducive to the evaluation and analysis in the actual environment. The lithium-ion battery equivalent model is simple to construct, has a smaller calculation volume, and can add correction factors to improve the accuracy of the model and facilitate its application in complex environments[26].

Power lithium-ion battery calculations usually rely on other battery parameters for constraints and feedback. Battery characteristics vary with temperature and charge/discharge conditions[27, 28]. A new polarization voltage model based on current and time to achieve accurate prediction for t=10s was proposed by Lin et al[29]. Lai, Xin proposed a fractional-order model-based SOP estimation scheme to achieve reliable estimation for dynamic conditions by segmentation analysis of different SOC stages[30]. Liu et al. used the capacity-temperature and resistance-temperature relationships from experimental data to more accurately predict the battery capacity and resistance over the entire temperature range, and used a multi-constraint algorithm to accomplish a reliable prediction over a wide temperature range[31]. Xiang, Shun et al. proposed a new fast method for calculating peak power with multiple constraints to achieve a constrained analysis of the battery state[32]. However, the above models only analyze the battery state under stable ambient temperature conditions, and it is difficult to track the representation of the internal characteristics of the battery in complex environments.

It is worth mentioning that at this stage, the description of the state of the battery SOP as a popular research point is often related to the material and internal state of the battery [33, 34]. In contrast, small

single lithium-ion batteries tend to fluctuate in measurement and control due to the shortcomings of their material properties [35] [36]. This study creatively introduced an improved algorithm that can track the description of the battery state and correct the effect of battery measurement errors [37]. It also constructs a method that can achieve effective tracking of the battery output state over a long period by characterizing the battery measurement data synchronously. The main advantages are as follows: (i) The overall structure is simple, the computational complexity is low, and the parameter tracking effect is better; (ii) The algorithm saves a lot of preliminary synchronous measurement time and reduces the testing cycle of the using manufacturer.

Based on the previous work, an online power state tracking estimation method is proposed under the constraint of a fusion model for powered lithium-ion batteries considering temperature effects in this study. The method obtains real-time parameters related to the temperature response by using an Improved Adaptive Forgetting Factor Recursive Least Squares(IAFFBCRLS) Method with Bias Compensation, which avoids the errors caused by multiple repeated experiments. Secondly, this paper improves the estimation accuracy of the fusion model by analyzing the capacity relationship of the power lithium-ion batteries with temperature change and correcting the battery capacity. Finally, the power representation of the battery is further tracked by constructing a fusion model with voltage, current and charge state as the influencing factors.

2. MATHEMATICAL ANALYSIS

2.1. Lithium-ion battery modeling

The reliability and workability of the power lithium-ion battery model is a prerequisite for characterizing the internal state of the lithium-ion battery. Generally speaking, the higher-order battery model has more accurate battery property characterization. In fact, the accuracy improvement brought by the higher-order model does not appear to be of large magnitude. This study analyzes the SOP algorithm based on the fusion model with the influence of multiple parameters, and the use of higher-order models undoubtedly introduces higher-order complexity matrices, which makes the calculation complex and increases the computational time. Therefore, considering the accuracy and complexity of the lithium-ion battery model, the Thevenin model is chosen to demonstrate the internal resistance and capacitance characteristics of the battery, as shown in Fig. 1.

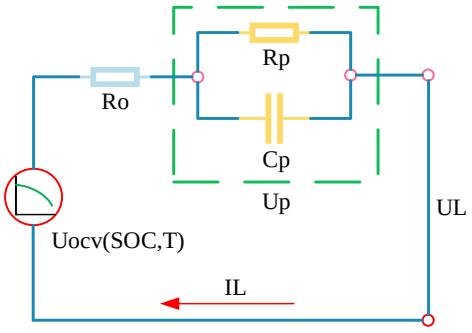

Figure 1. The Thevenin equivalent circuit model

Among them, the battery model shown in Fig. 1 is divided into four main parts: (i) *Uocv(SOC,T)* characterizes the battery terminal voltage under the influence of temperature and SOC; (ii) *Ro* characterizes the ohmic resistance of the battery; (iii) *Rp* and *Cp* together characterize the polarization effect of the battery, with *Rp* representing the polarization resistance of the battery and *Cp* representing the polarization capacitance of the battery; (iv) *UL* characterizes the battery voltage of the battery under load conditions. In addition, *Up* characterizes the polarization voltage of the battery, and *IL* represents the discharge or charging current of the battery.

Thus, the equivalent circuit model can be expressed as

$$\begin{cases} \chi_k = A_{k-1}\chi_k + B_{k-1}IL_{k-1} \\ UL_k = Uocv(SOC,T)_k - Ro_k IL_k - Up_k \end{cases} \tag{1}$$

Among them

$$\begin{cases} \chi_k = [Up_k \quad SOC_k]^T \\ A_{k-1} = \begin{bmatrix} \varepsilon_{k-1} & 0 \\ 0 & 1 \end{bmatrix} \\ B_{k-1} = \begin{bmatrix} Rp_{k-1}(1-\varepsilon_{k-1}) & \dfrac{t}{3600Qc(T)} \end{bmatrix}^T \\ \varepsilon_{k-1} = e^{\frac{-t}{Rp_{k-1}Cp_{k-1}}} \end{cases} \tag{2}$$

Where *k* denotes the state of each stage, *t* denotes the sampling time, and *Qc(T)* denotes the battery capacity at the current temperature. The matrix superscript *T* only indicates the mathematical transposition effect, which is not related to the temperature. The internal resistance and capacity characteristics of the battery under complex temperature conditions are often difficult to obtain for analysis. In this study, the capacity characteristics of the battery under the influence of variable temperature are analyzed in advance, and the reliable analysis of the battery characteristics is accomplished by full-parameter online parameter identification.

2.2. Online parameter identification based on IAFFBCRLS

Parameter identification usually relies on further coupling analysis of the intrinsic properties between voltage and current. Off-line parameter identification is often performed by performing a large number of a priori analyses to obtain a reliable fitted characterization of multiple factors that may affect the internal state of the battery. Such an approach has a long time cycle and weak dynamic response, which is not conducive to the rapid industrial application of power lithium-ion batteries. The accurate representation of online parameters depends on the selection of the battery model and the effective tracking of the algorithm. The least squares based online identification of power lithium-ion batteries with data preprocessing is shown in Fig. 2.

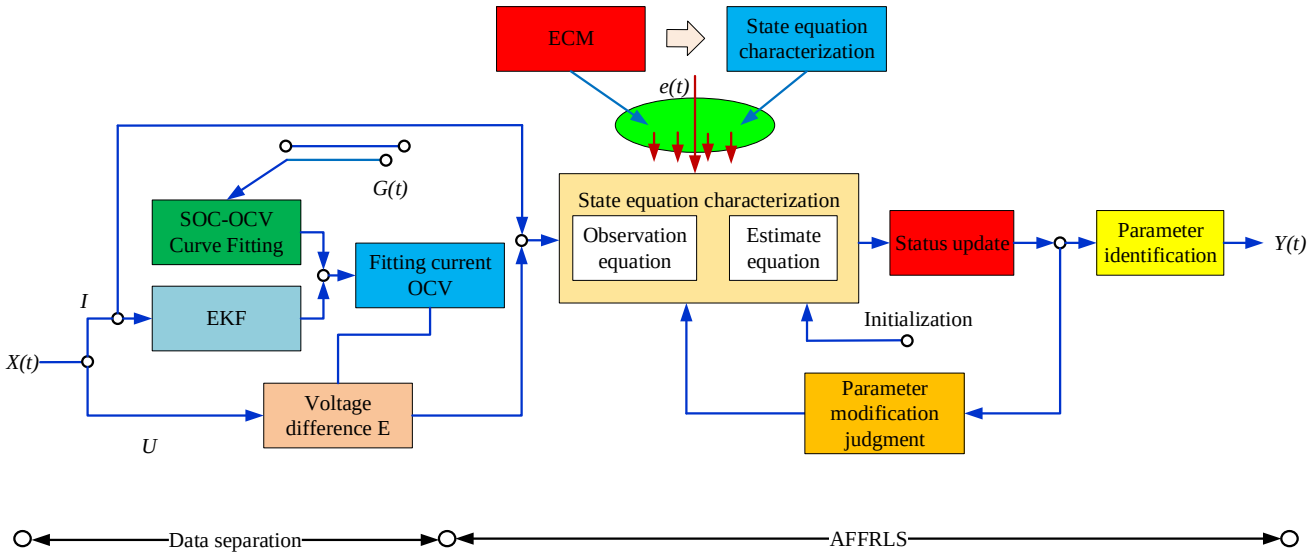

Figure 2. Flow chart of online parameter identification with data pre-processing

Among them, *X(t)* represents the dynamic operating state of the battery, including the voltage and current of the battery; *G(t)* represents the battery state under constant current discharge, which is generally composed of the battery voltage and SOC obtained from the HPPC work analysis; *Y(t)* represents the parameters under online parameter identification (the parameter type is determined by the battery model), and *e(t)* represents the system error. The specific process of converting the equivalent circuit model of a lithium-ion battery to least squares is shown in Fig. 3.

Where *Uocv(SOC)* represents the voltage value obtained by the battery from the SOC-OCV curve fitting relationship analysis of the current SOC, *T* represents the sampling time of the battery. It is easy to see that the basis of the algorithm analysis is to pre-process the voltage of the battery, to analyze the coupling relationship between the battery voltage and current, and thus obtain the state parameters of the battery at each moment. The power lithium-ion battery is in a complex operating environment, and the internal relationship between its SOC and OCV is difficult to obtain. Online identification with data preprocessing needs to rely on a priori experimental data and data preprocessing optimization at the input side, which not only brings a large number of early calculations but also introduces new errors.

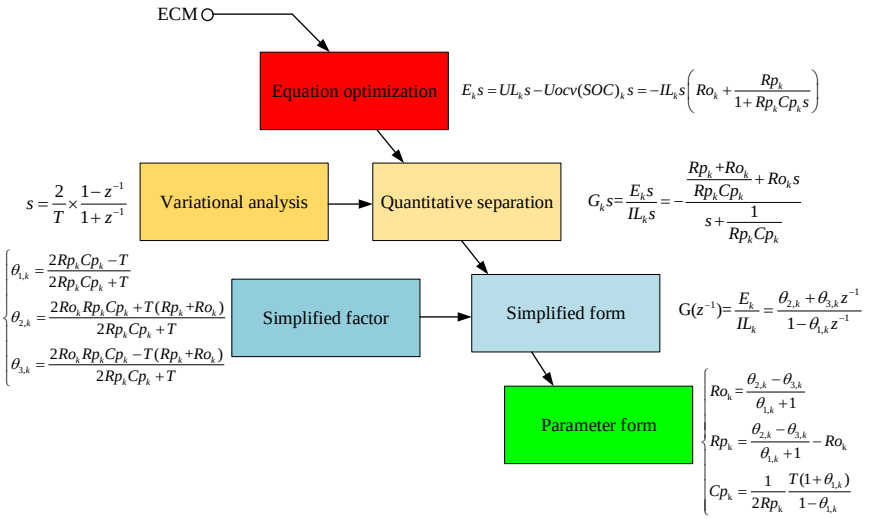

Figure 3. Flow chart of model squares change with data pre-processing

This study discards the traditional external SOC-OCV curve fitting analysis of online parameter identification and considers the influence of ambient temperature to construct a full-parameter online identification method for adaptive tracking of battery OCV curve based on the influence of temperature. (i) Simultaneous analysis is performed by separating the parameters and treating *Uocv* as an unknown quantity; (ii) The influence of ambient temperature is introduced to impose a correction effect to obtain the best-coupled representation of the internal factors for real-time estimation of the battery parameters. Extending the matrix representation to separate the influence voltage variable *Uocv*, the optimization part of the equation in Fig. 3 can be rewritten as the matrix expression shown in Eq. 3.

$$\begin{cases} UL_2 = Uocv_2 + \theta_{1,1} Uocv_1 + \theta_{1,1} UL_1 + \theta_{2,1} IL_2 + \theta_{3,1} IL_1 + e_1(k) \\ UL_3 = Uocv_3 + \theta_{1,2} Uocv_2 + \theta_{1,2} UL_2 + \theta_{2,2} IL_3 + \theta_{3,2} IL_2 + e_2(k) \\ \vdots \quad \vdots \quad \vdots \quad \vdots \quad \vdots \\ UL_k = Uocv_k + \theta_{1,k-1} Uocv_{k-1} + \theta_{1,k-1} UL_{k-1} + \theta_{2,k-1} IL_k + \theta_{3,k-1} IL_{k-1} + e_{k-1}(k) \end{cases} \tag{3}$$

Where θ represents the coupling factor of the battery parameters. By introducing new variables and simplifying the matrix representation (without interference terms in Eq.), the representation of the cell characteristics throughout the study phase is analyzed, as shown in Eq. 4.

$$\begin{cases} U_{L,k} = \varphi_k \sigma_k^T \\ \varphi_k = [1 \quad UL_{k-1} \quad IL_k \quad IL_{k-1}] \\ \sigma_k = [Uocv_k + \theta_{1,k-1} Uocv_{k-1} \quad \theta_{1,k-1} \quad \theta_{2,k-1} \quad \theta_{3,k-1}] = [\sigma_{1,k} \quad \sigma_{2,k} \quad \sigma_{3,k} \quad \sigma_{4,k}] \end{cases} \tag{4}$$

Where φk is the observed vector and $б k$ is the parameter vector to be estimated. However, due to the errors and noise interference of the measurement instruments in complex operating conditions, it is inevitable to cause errors in the acquisition of battery data (current and voltage). Therefore, Eq. 4 can be discussed separately for voltage and current, as shown in Eq. 5.

$$\begin{cases} UL_k = UL_{k,0} + \tilde{U}L_k \\ IL_k = IL_{k,0} + \tilde{I}L_k \end{cases} \tag{5}$$

Where $UL_{k,0}$ denotes the voltage reference value collected at moment k; $\tilde{U}L_k$ denotes the voltage value applied by the error disturbance at moment k; similarly, $IL_{k,0}$ denotes the current reference value collected at moment k; $\tilde{I}L_k$ denotes the current value applied by the error disturbance at moment k. The object of the algorithm consideration is the tracking effect of the voltage. Therefore, the voltage is considered as the output and the current is considered as the input. The sources of error against the battery data can be represented in Fig. 4.

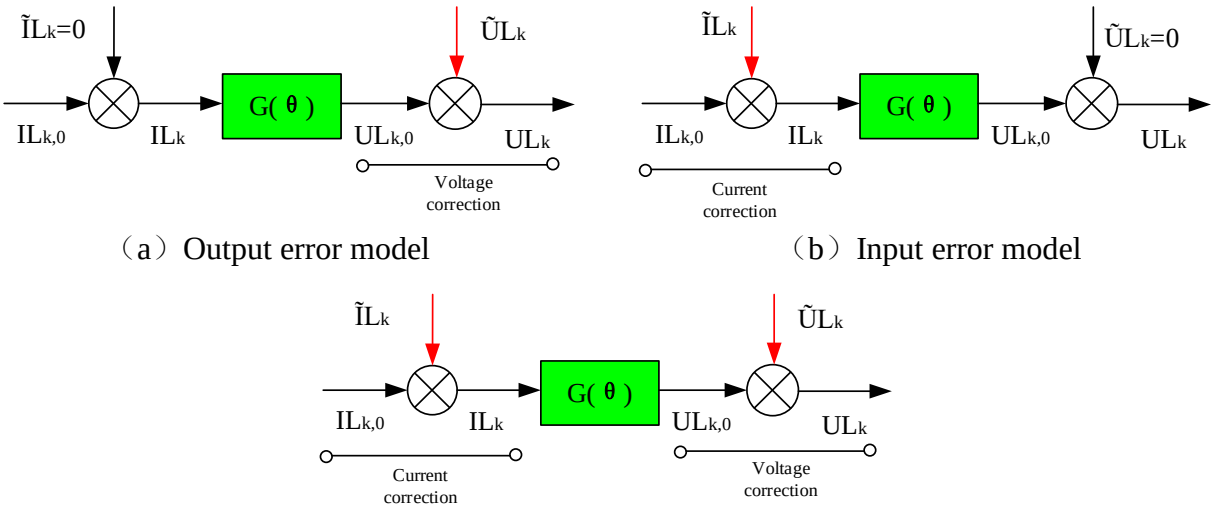

Figure 4. Model analysis of data error sources

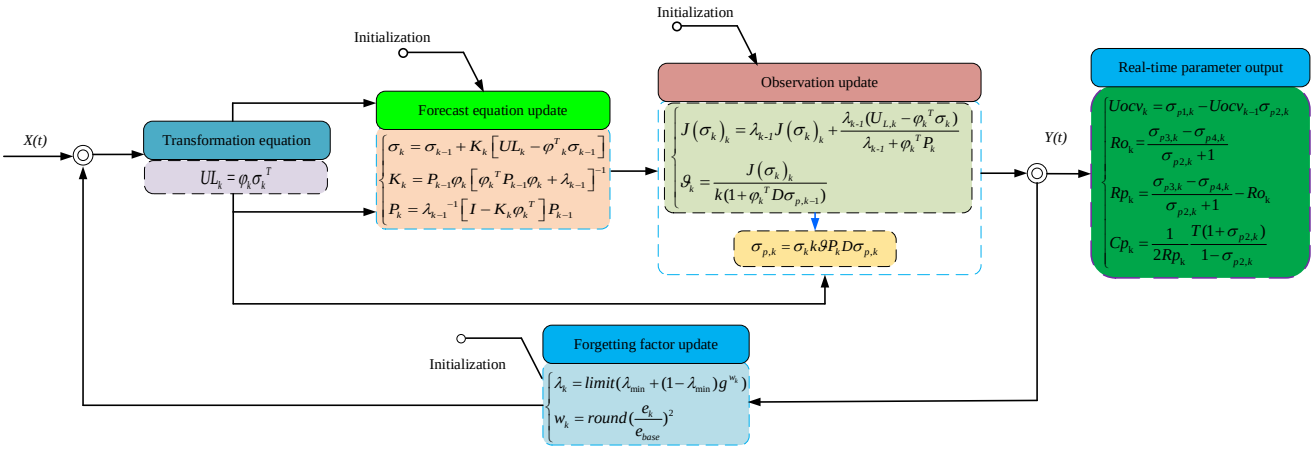

Figure 5. The flow chart of the IAFFBCRLS algorithm

Among them, $\tilde{I}L_k=0$ and $\tilde{U}L_k\neq0$ are considered as the output error model; $\tilde{I}L_k\neq0$ and $\tilde{U}L_k=0$ are considered as the input error model; $\tilde{I}L_k\neq0$ and $\tilde{U}L_k\neq0$ are considered as the double error model. For the improved algorithm is used in the battery voltage, the SOC-OCV curve is not introduced to assist in

fitting, so the battery state parameters that are under the influence of the output error are mainly considered in the study. As a result, a better coupling, better robustness, and better accuracy of the battery operating parameters characterization are obtained by continuous correction of the data. The flow chart of the IAFFBCRLS algorithm is shown in Fig. 5.

Wherein, *X(t)* denotes the experimental data to be analyzed for the power lithium-ion battery; *Y(t)* denotes the online parameter identification data of the power lithium-ion battery obtained by analyzing the working condition characteristics. The following description is provided for the specific implementation of the algorithm.

(i) Conversion equation: The matrix analysis characterization of the continuous response is constructed by analyzing the internal coupling relationship of the battery under the influence of the output error and analyzing the battery voltage (combining Eq. 4 and Eq. 5).

(ii) Updating of the prediction equation: First, the parameter vector $б$ to be estimated without the disturbance of the error is estimated by pairing the matrix gain K; then, the forgetting factor λ and the matrix covariance P are introduced to update K; finally, P is updated by updating the gain K and the forgetting factor λ.

(iii) Observation update: First, the residual J is obtained from the tracking representation without error disturbance to evaluate the algorithm correction effect; second, the evaluation factor ϑ is introduced to evaluate the noise error; finally, the parameter vector $бp$ under the influence of error disturbance is obtained by analyzing the relationship between each coupling parameter. Where D denotes the error disturbance influence matrix, k denotes the sampling time.

(iv) Forgetting factor update: By analyzing the state representation under the error disturbance, the correction effect of voltage and other parameters is judged, so that the forgetting factor λ can be continuously corrected to strengthen the correction effect or weaken the over-correction to achieve a reliable and effective tracking of the parameters. Where λmin denotes the minimum value of the forgetting factor, which is generally set to 0.96~1; *limit* denotes the restriction on the observed object; g denotes the correction sensitivity coefficient to indicate the sensitivity of the forgetting factor to large errors and strengthen its correction effect, which is generally set to 0~1; w denotes the ratio relationship between the observed quantity and the reference quantity; e_k denotes the value of the observed quantity at time k; and e_{base} denotes the reference quantity, which is usually set to the value of the desired correction effect; *round(x)* denotes the integer value closest to x, which is used to attenuate the overfitting caused by small errors.

(v) Real-time parameter output: Combined with the above process, the real-time lithium-ion battery parameter characteristics are obtained by decoupling the relationship of the parameter vector $бp$ under the influence of error disturbance.

In summary, the IAFFBCRLS algorithm can track the equivalent model parameter representation of the internal chemical properties by analyzing the external battery characteristics (voltage and current) and correct the errors caused by the battery voltage separation. Compared with the IAFFRLS algorithm with data pre-processing, the process of pre-experimental analysis and data processing is circumvented, the adaptability and operability of the algorithm is improved effectively.

2.3. State of Power estimation under fusion algorithm

Power lithium-ion batteries usually rely on packs to achieve high energy output. The inconsistency of SOC in use for each battery will affect the high or low battery voltage. A single limit can guide the power output range of a battery. However, for packaged batteries, the capacity of each pack is different, and the battery characteristics of the battery under the same duration are more variable, so a single limit often outputs a reference amount without practical meaning, which in turn causes a large difference in the power epithet of a single battery.

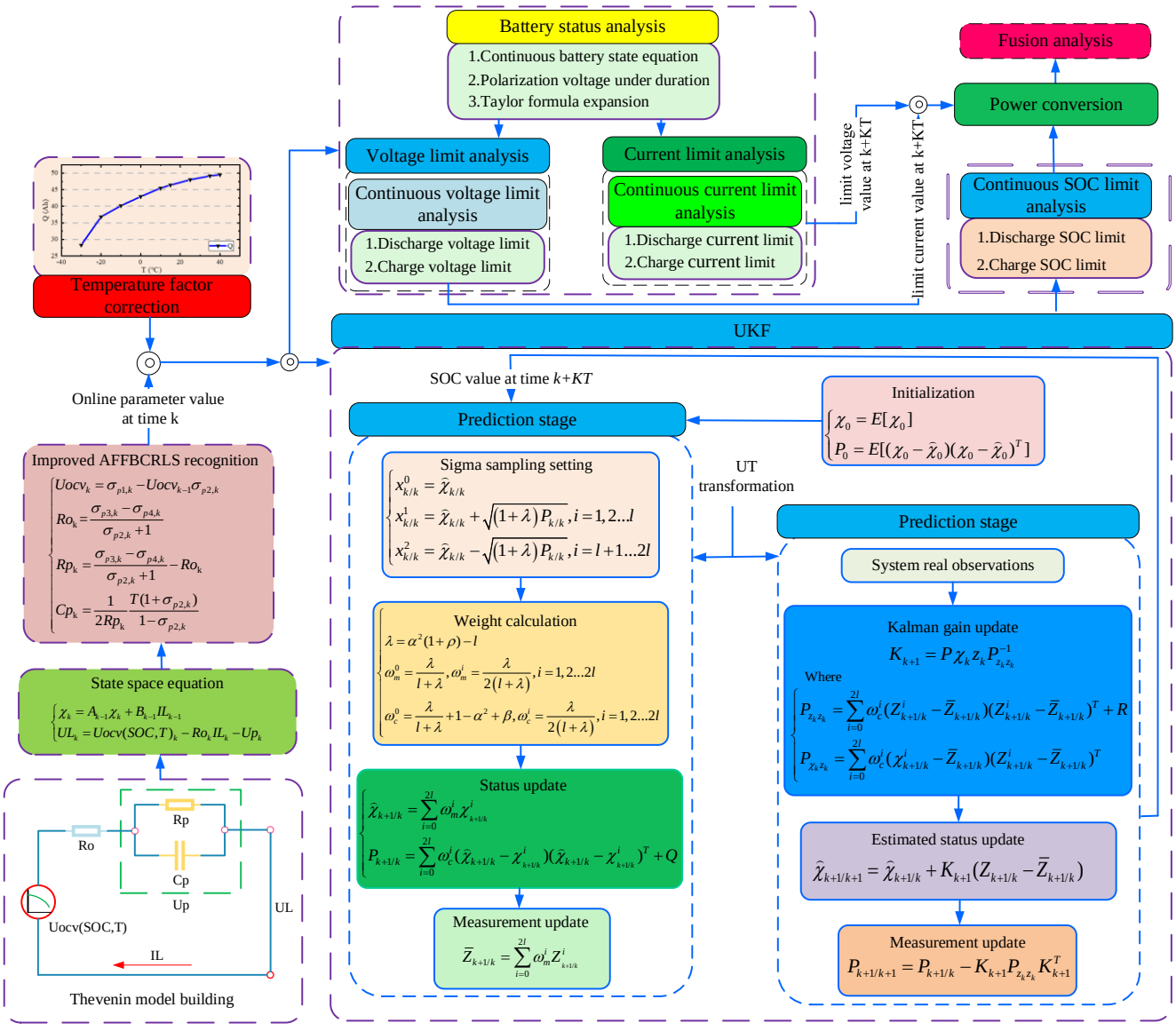

Figure 6. SOP estimation method with temperature-corrected fusion model limits

Accurate estimation of SOP can achieve efficient power distribution, effectively avoid overcharge and over-discharge of batteries, and extend the life of power lithium-ion battery packs. Maintaining the peak operation of electric vehicles for a longer period is the basis of the analysis.

Therefore, this paper investigates the state output characteristics of vehicle operation under continuous-time and proposes the SOP estimation method with fusion model limits containing temperature correction, as shown in Fig. 6.

As shown in Fig. 6, the SOP algorithm is divided into three main parts. First, the IAFFBCRLS algorithm provides high-precision and real-time online parameter data for the model; Second, the UKF algorithm provides the effect of temperature change by introducing the curve fitting equation for the temperature change to achieve a reliable prediction of the temperature effect; Finally, the power output under the fusion model is analyzed by introducing online parameter identification and temperature effects with current, voltage and SOC constraints.

The fusion model analysis method for temperature correction effects is further described for the above-related estimation process. Considering the state of each moment individually is not of practical application. The following assumes that its peak current is constant at a sampling time *KT*. Parameter states of power lithium-ion batteries can be represented by Eq. 6.

$$\begin{cases} \chi_{k+K_T} = A_k^{K_T} + (\sum_{n=1}^{K_T} A_k^{n-1} B_k) IL_k \\ UL_{k+KT} = Uocv(SOC,T)_{k+KT} - Ro_k IL_{k+KT} - Up_{k+KT} \end{cases} \tag{6}$$

The characteristics of the polarization voltage and the battery terminal voltage over the duration are expressed as Eq. 7.

$$\begin{cases} Up_{k+K_T} = Up_k e^{\frac{-K_T}{Cp_k Rp_k}} + (1 - e^{\frac{-K_T}{Cp_k Rp_k}}) Rp_k IL_{k+K_T} \\ Uocv(SOC,T)_{k+KT} = Uocv(SOC,T)_k - \dfrac{\eta K_T}{Qc(T)} \dfrac{\partial Uocv(SOC,T)_k}{\partial SOC_k} IL_{k+K_T} \end{cases} \tag{7}$$

According to the above, *Uocv(SOC,T)* is the real-time voltage data obtained by relying on the IAFFBCRLS algorithm. Where the derivative operation is obtained by simultaneous fitting of *Uocv(SOC,T)* to the SOC relationship according to a single sampling. Where η is the Coulomb coefficient; *Qc(T)* is obtained by fitting the capacity relationship curve influenced by the temperature factor. Therefore, the battery load voltage can be obtained by combining Eq. 6 and Eq. 7, as shown in Eq. 8.

$$\begin{aligned} UL_{k+K_T} = {} & OCV(SOC,T)_k - Up_k e^{\frac{-K_T}{Cp_k Rp_k}} \\ & - IL_{k+K_T} [\frac{\eta K_T}{Q_c(T)} \frac{\partial OCV(SOC,T)_k}{\partial SOC_k} + Ro_k + (1 - e^{\frac{-K_T}{Cp_k Rp_k}}) Rp_k] \end{aligned} \tag{8}$$

However, the observable voltage of a power lithium-ion battery is limited. The open-circuit voltage of the battery at any moment should satisfy the charging or discharging limit. Therefore, the continuous peak charging or discharging current of the battery at the voltage limit can be expressed as Eq. 9.

$$\begin{cases} I^{V}_{dis,k+K_T} = -\dfrac{v_{\min} - Uocv(SOC,T)_{k+KT} + Up_k e^{\frac{-K_T}{Cp_k Rp_k}}}{\dfrac{\eta K_T}{Q_c(T)}\dfrac{\partial Uocv(SOC,T)_k}{SOC_k} + Ro_k + Rp_k(1-e^{\frac{-K_T}{Cp_k Rp_k}})} \\ I^{V}_{cha,k+K_T} = -\dfrac{v_{\max} - Uocv(SOC,T)_{k+KT} + Up_k e^{\frac{-K_T}{Cp_k Rp_k}}}{\dfrac{\eta K_T}{Q_c(T)}\dfrac{\partial Uocv(SOC,T)_k}{SOC_k} + Ro_k + Rp_k(1-e^{\frac{-K_T}{Cp_k Rp_k}})} \end{cases} \quad (9)$$

Among them, $I^{V}_{dis,k+KT}$ is the peak current that the battery can reach in a continuous discharging state under-voltage limitation; $I^{V}_{cha,k+KT}$ is the peak current that the battery can reach in a continuous charging state under-voltage limitation; v_{min} is the discharge cutoff voltage (related to the measurement settings); v_{max} is the charge cutoff voltage (related to the battery characteristics). By analyzing the changes in the state of the battery parameters in real-time, it is possible to analyze the current representation under the limit and, consequently, the power representation.

In the same way, power lithium-ion batteries are currently limited due to their material composition. Current limiting means limiting the value by metering the output voltage through the peak battery current at a constant duration. Thus, the continuous charge or discharge voltage based on current limitation can be expressed as Eq. 10.

$$\begin{cases} V^{I}_{dis,k+K_T} = Uocv(SOC,T)_{k+KT} + Up_k e^{\frac{-K_T}{Cp_k Rp_k}} - \\ \qquad i_{dis}\left(\dfrac{\eta K_T}{Q_c(T)}\dfrac{\partial Uocv(SOC,T)_k}{SOC_k} + Ro_k + Rp_k(1-e^{\frac{-K_T}{Cp_k Rp_k}})\right) \\ V^{I}_{cha,k+K_T} = Uocv(SOC,T)_{k+KT} + Up_k e^{\frac{-K_T}{Cp_k Rp_k}} - \\ \qquad i_{cha}\left(\dfrac{\eta K_T}{Q_c(T)}\dfrac{\partial Uocv(SOC,T)_k}{SOC_k} + Ro_k + Rp_k(1-e^{\frac{-K_T}{Cp_k Rp_k}})\right) \end{cases} \quad (10)$$

Where $V^{I}_{dis,k+KT}$ is the peak current that the battery can reach when it is in a continuous discharge state under the current limit; $V^{I}_{cha,k+KT}$ is the peak current that the battery can reach when it is in a continuous charge state under the current limit; idis denotes the maximum peak discharge current that the battery can provide under the continuous state; icha denotes the maximum peak charging current.

In addition, the battery SOC can reflect the safety and reliability of the battery. For the reliable operation of electric vehicle battery pack, the lithium-ion battery SOC needs to be limited, i.e., $SOCmin \geq SOCk \geq SOCmax$. Under the current SOC limit, the peak discharge and charge currents of lithium-ion batteries are expressed in Eq. 11.

$$\begin{cases} I^{SOC}_{dis,k+K_T} = \dfrac{SOC_k - SOC_{\min}}{\eta K_T / Q_c(T)} \\ I^{SOC}_{cha,k+K_T} = \dfrac{SOC_k - SOC_{\max}}{\eta K_T / Q_c(T)} \end{cases} \quad (11)$$

The $I^{SOC}_{dis,k+KT}$ is the peak current that can be achieved when the battery is in a continuous discharge state under the SOC limit; $I^{SOC}_{cha,k+KT}$ is the peak current that can be achieved when the battery

is in a continuous charge state under the SOC limit; the voltage and current of the power lithium battery fluctuate greatly at low SOC, making it difficult to provide a reliable reference quantity. The SOC limit enables to the analysis of the power representation of the battery at low SOC and achieves a reliable power output representation for the full sampling period.

In summary, the battery power state characterization under the fusion model can be obtained as shown in Eq. 12.

$$\begin{cases} P_{dis,k+K_T} = min(v_{min}I^{V}{}_{dis,k+K_T},\ v_{min}I^{SOC}{}_{dis,k+K_T}, idisV^{I}{}_{dis,k+K_T}) \\ P_{cha,k+K_T} = max(v_{max}I^{V}{}_{cha,k+K_T},\ v_{max}I^{SOC}{}_{cha,k+K_T}, ichaV^{I}{}_{cha,k+K_T}) \end{cases} \quad (12)$$

Where, $P_{dis,k+KT}$ represents the battery discharge SOP under-voltage limit discharge. $P_{cha,k+KT}$ represents the battery discharge SOP under-voltage limit charge. By constructing the peak output power estimation system with different durations, the battery characteristics under different states are analyzed, which provides a reliable data reference for users.

Therefore, this paper proposes an online power state tracking estimation method under the constraints of a fusion model for lithium-ion batteries that considers the effects of temperature. Wei et al proposed an extreme value seeking algorithm to identify the parameters of the battery, and then based on the circuit model to determine the parameters, considering the voltage and current limits of the battery, finally obtained the SOP[37]. Esfandyari et al proposed a hybrid control system based on model prediction and fuzzy logic to estimate the SOP of the battery[38]. Compared to these algorithms, an improved adaptive forgetting factor recursive least squares method is used to obtain real-time parameters related to temperature on each experiment, and the capacity of the power lithium-ion battery is analyzed by temperature variation and corrected for it, thus improving the estimation accuracy of the fusion model with voltage, current and state of charge as influencing factors and further tracking its power.

3. EXPERIMENTAL ANALYSIS

3.1. Test platform construction and data analysis

Quantitative analysis of the battery state is the basis for describing the changes in its internal characteristics. Reliable analysis of lithium-ion batteries cannot be achieved without the support of reliable data measured by instruments. The study was tested using 26650 cells (the research object shown in Fig. 7 is for demonstration purposes only and is not relevant in practice). The temperature test environment uses a three-field independent temperature control box (BT-331C), and the data acquisition equipment is a high-power charge/discharge tester (CT- 4016-5V100A-TFA) for power lithium-ion batteries. The test flow of the research object is shown in Fig. 7.

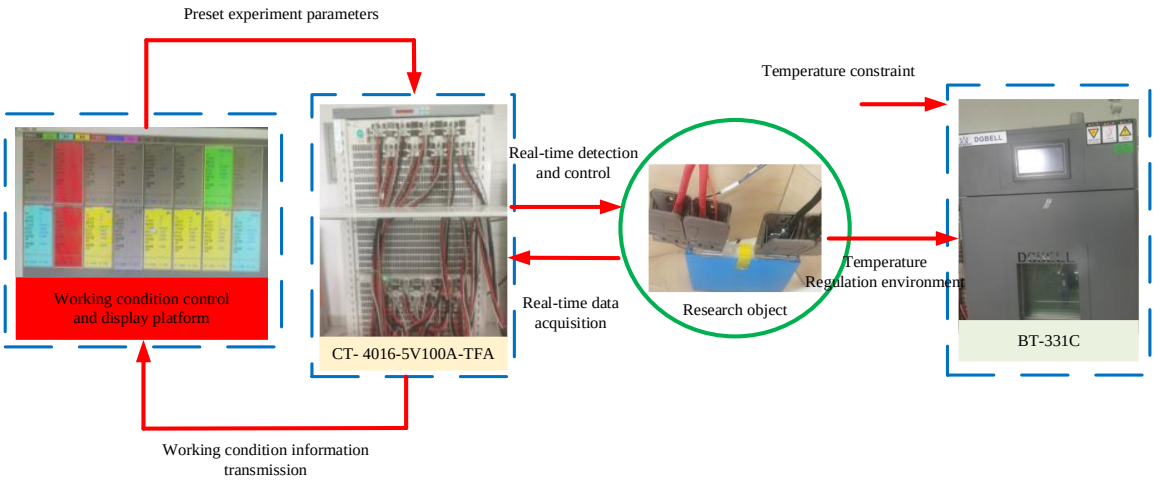

Figure 7. The test flow of the research object

The characteristics of lithium-ion batteries at complex temperatures are complex and changeable. The researchers constructed the battery pulse discharge test at different stages at -5℃, 5℃, 10℃, 25℃ and 35℃, the change in the capacity of the power lithium-ion battery under the influence of temperature is shown in Fig. 8.

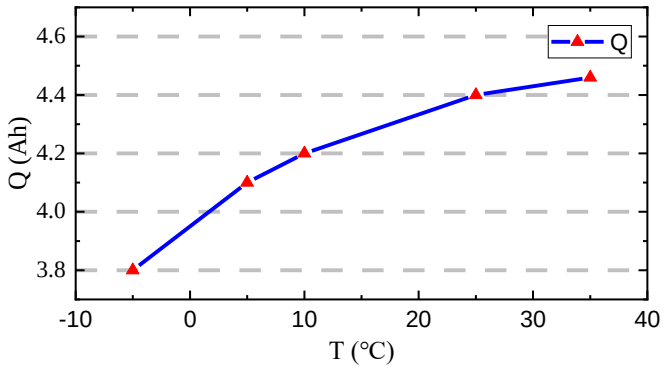

Figure 8. The change in the capacity of the power lithium-ion battery under the influence of temperature

As can be seen from the above figure, the battery capacity decreases as the temperature decreases. When the temperature is lower than 5℃, as the ambient temperature drops, the battery capacity will fall off a cliff; When the battery temperature is higher than 25℃, within a safe range, as the temperature rises, the battery capacity tends to a stable value. Therefore, in the face of the battery status under complex temperature conditions, its internal parameters and external characteristics are difficult to predict.

Therefore, based on the temperature change curve, a polynomial can be constructed to represent the battery capacity as shown in Tab. 1.

Table 1. Capacity curve fitting based on temperature variation

$Q(T)=aT^4+bT^3+cT^2+eT+f$				
a	b	c	d	f
-2.444e-7	1.967e-5	-8.328e-4	2.951e-2	3.971

This method can solve the interference brought to the algorithm by the fluctuation of battery capacity under the temperature perturbation. However, for the complex external working environment, the measurement accuracy of the temperature sampling device of the device also inevitably brings interference.

3.2. Online parameter identification under continuous pulse conditions

The identification of lithium-ion battery parameters is the basis for conducting subsequent studies. The battery states of different batches of lithium-ion batteries are inconsistent. Therefore, in this paper, different batches of lithium-ion batteries are selected for the single BBDST discharge test to verify the adaptability of the improved algorithm. In which, setting discharge power of each battery is consistent and is tested at the same constant temperature.

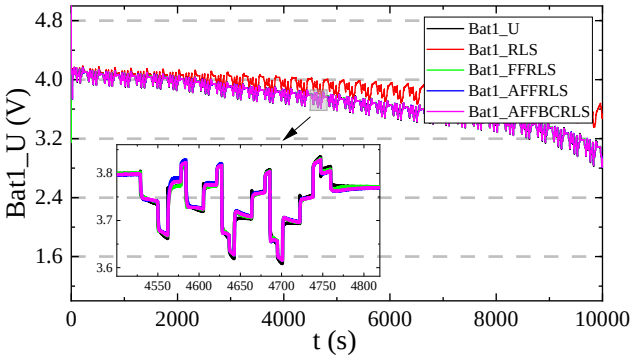

(a) Voltage fitting of single battery 1 based on different algorithms

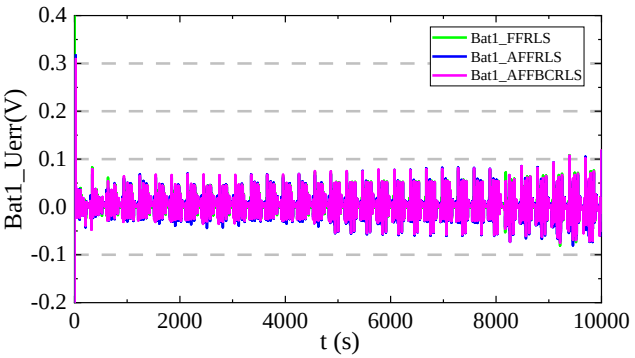

(b) Voltage error of single battery 1 based on different algorithms

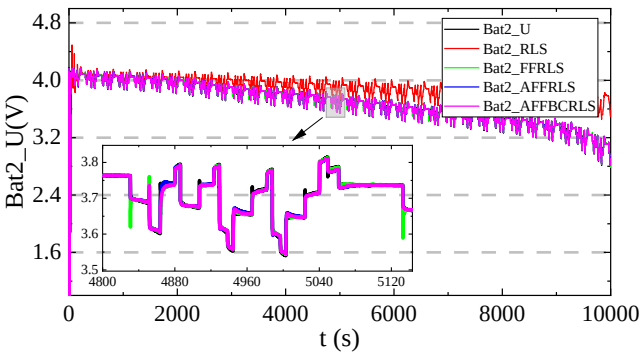

(c) Voltage fitting of single battery 2 based on different algorithms

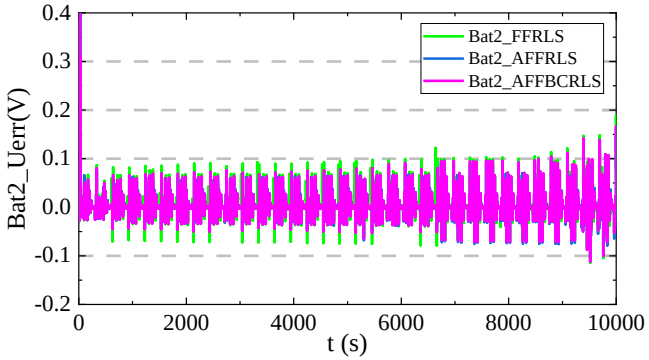

(d) Voltage error of single battery 2 based on different algorithms

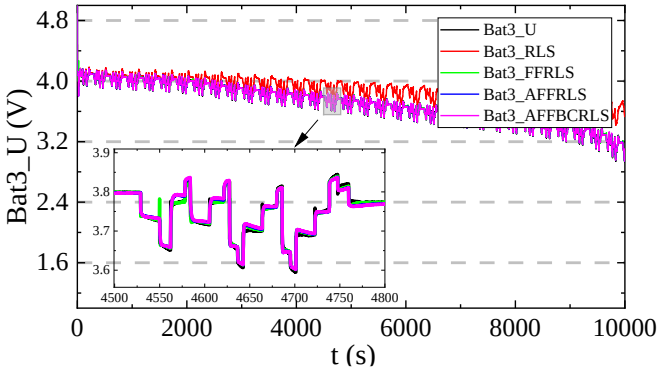

(e) Voltage fitting of single battery 3 based on different algorithms

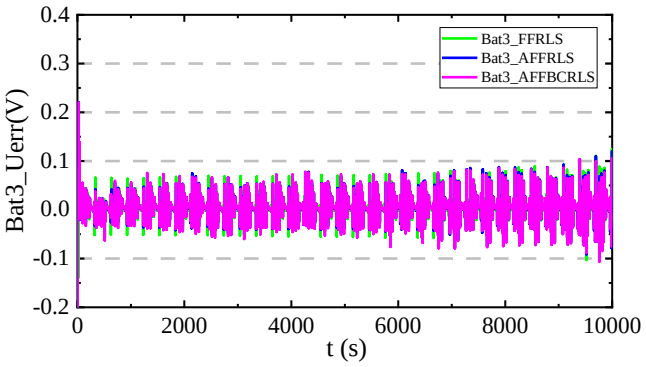

(f) Voltage error of single battery 3 based on different algorithms

Figure 9. The effect of the lithium-ion battery algorithm tracking algorithm

All algorithms are used the matrix resolution method to analyze the battery voltage away from and analyze the battery parameter state and OCV simultaneously. The tracking effect of this algorithm of lithium-ion battery is shown in Fig. 9.

Where *U* denotes the reference voltage value collected by the test instrument; *RLS* denotes the voltage of the parameter identification feedback using the RLS algorithm; *FFRLS* denotes the voltage of the parameter identification feedback using the FFRLS algorithm (λ=0.99); *AFFRLS* denotes the voltage of the parameter identification feedback using the AFFRLS algorithm (λmin=0.98); AFFBCRLS denotes the voltage of the parameter identification feedback using the AFFBCRLS algorithm(λmin=0.98, D=[0 0.1 1 1]). The AFFRLS algorithm has a good fit analysis for the voltage rise phase, but overfitting can occur. The correction accuracy of AFFRLS is significantly lower than that of AFFBCRLS algorithm. Therefore, the AFFBCRLS algorithm has better correction and better analysis of the discharge process under different single-cell test application conditions.

The tracking effectiveness of other parameters of the battery characteristics is also an important consideration. The specific tracking performance of the IAFFBCRLS algorithm is illustrated below with a single battery 2 for verification. It is worth mentioning that due to the difficulty of maintaining constant power discharge of the battery at the end of discharge, the voltage of the battery drops too fast and will reach the cutoff voltage instantaneously, which make it difficult to consider the analysis. Therefore, only the operating characteristics of the battery at the first 90% SOC are analyzed. The external characteristics of the power lithium-ion battery are shown in Fig. 10.

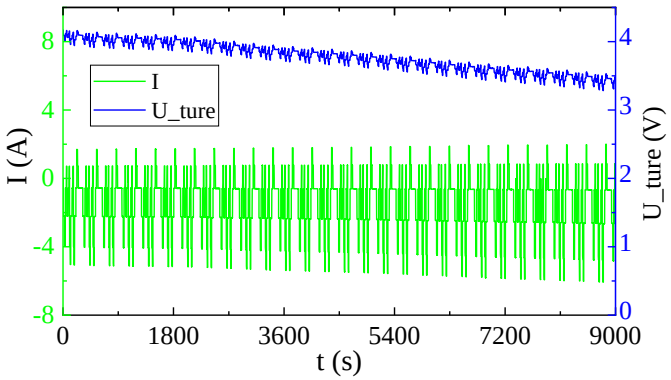

Figure 10. The external characteristics of the power Li-ion battery

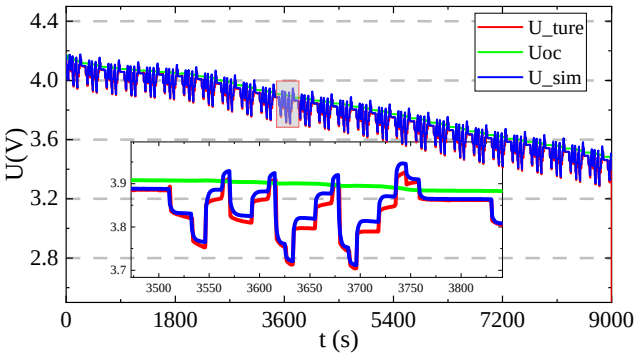

(a) Voltage simulation curve based on IAFFBCRLS algorithm

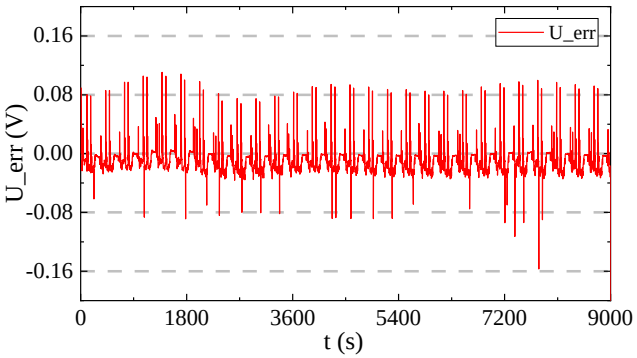

(b) Voltage error curve based on IAFFBCRLS algorithm

Figure 11. The voltage simulation and error based on the IAFFBCRLS algorithm

From the above graph, while it can be seen that as the battery voltage decreases, there is a significant increase in the current at constant power output. So with the help of this experiment to describe the characteristics of the battery is beneficial to analyze, the power output of the battery. The voltage simulation and error based on the IAFFBCRLS algorithm are shown in Fig. 11.

The voltage tracking curve is the basis for describing the battery characteristics. Among them, *U_ture* indicates the effective sampling data of the battery; *U_sim* and *Uoc* are the voltage simulation value and open-circuit voltage simulation value obtained based on the IAFFBCRLS algorithm respectively. From the figure, it can be seen that the performance of battery decoupling and battery simulation analysis based on the IAFFBCRLS algorithm is good, and the simulation error of the battery is lower than 0.08V, which can be effectively tracked and analyzed for the battery. The resistance and capacitance characteristics of the battery based on the IAFFBCRLS algorithm are represented in Fig. 12.

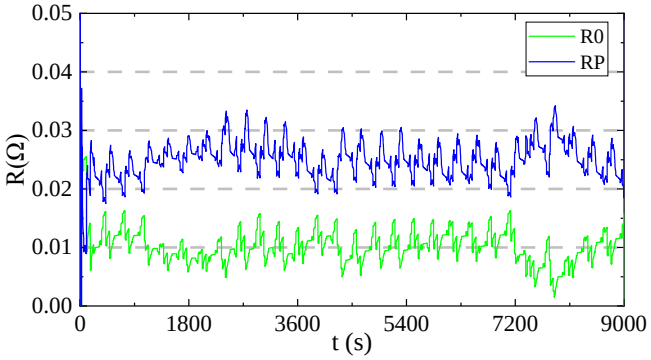

(a) Resistance characteristics based on IAFFBCRLS algorithm

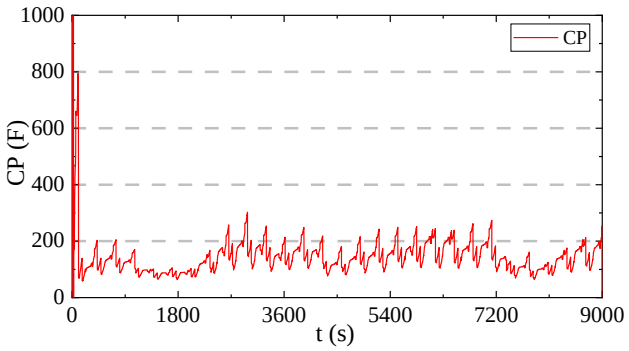

(b) Capacitance characteristics based on IAFFBCRLS algorithm

Figure 12. The resistance and capacitance characteristics of the battery based on the IAFFBCRLS algorithm

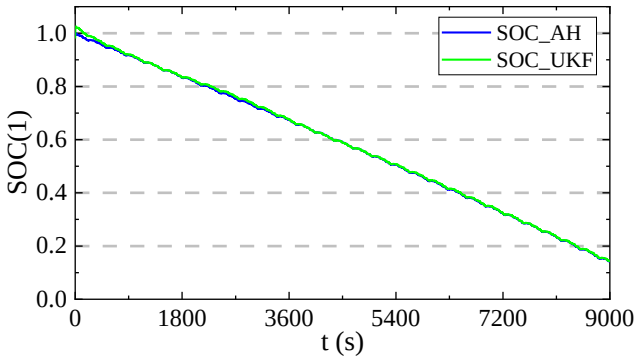

（a）SOC estimation curve based on UKF algorithm

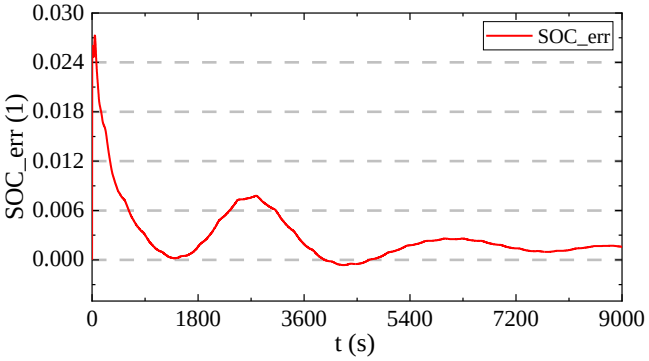

(b) SOC estimation error curve based on UKF algorithm

Figure 13. The SOC simulation curve by UKF algorithm

The reliability of the resistance and capacitance characteristics affects the effectiveness of the analysis for power output. The graph shows that the resistance and capacitance characteristics fluctuate. During the whole metering cycle, the ohmic resistance R_0 of the battery fluctuates around 0.01Ω for a long time; The polarization resistance R_P of the battery fluctuates around 0.025Ω, and the polarization capacitance of the battery varies around 150F. Therefore, the SOC simulation curve by expressing the influence of the above-mentioned parameter coupling and based on the UKF algorithm is shown in Fig. 13.

Apparently, the UKF algorithm coupled with online parameters can achieve a reliable prediction of SOC with an error of less than 0.5%. The method is composed based on the analysis of OCV curves obtained from online parameters and can provide reliable online SOC output for accurate estimation of SOP with reliable parameters.

3.3. Working condition demonstration effect

The battery power index of power lithium-ion batteries in commercial situations is an important reference for users. An accurate description of the battery power information is a prerequisite for algorithm verification. The traditional HPPC test treats the battery discharge as a whole as a resistive influence, which inevitably introduces a huge amount of interference and can cause the measured power to be significantly higher than the true value in a longer duration discharge. The following constant power method is used to test and analyze the battery power, as shown in Tab. 2.

Table 3. Constant power testing process

Taking 50% power output as an example, the specific process of power testing is as follows
(i) Place the object under test in a 25℃ thermostat and leave it for 2h;
(ii) Charge with 1C constant current to a cut-off voltage of 4.2V and constant voltage to a current less than 0.05C, and leave it for 1h;
(iii) Discharge the battery with 1C to adjust the SOC to 50% SOC and leave it for 1h;
(iv) apply constant power P discharge to the object under test, record the time T consumed by the discharge to the cut-off voltage (2.75V), judge whether the time consumed T is within the fitting judgment interval (T<=60s), and leave it for 1h;
(v) If T does not meet the judgment interval then fine-tune the power P and repeat (ii)~(iv) to make the time meet the judgment interval and record the power P and time T;
(vi) Repeat (ii) ~ (iv) to record at least three times.
(vii) Fit the power P and time T recorded each time and analyze the peak power output for different durations.

The time and power of a single cell battery discharged from the charge cutoff voltage to the discharge cutoff voltage becomes an important consideration. At this point, the power output characteristics of the single-cell battery are described as the power output that the battery can maintain from the fully charged state to the power cutoff within a set time is considered as the constant peak power output within the set time. The constant power test data of the single-cell battery is shown in Tab. 3.

Table 4. Constant power test data of single cell battery

SOC=1		SOC=0.9		SOC=0.8		SOC=0.7		SOC=0.6	
P(W)	T(s)	P(W)	T(s)	P(W)	T(s)	P(W)	T(s)	P(W)	T(s)
68	9.6	68	8	66	8.7	66	6.6	65	6
65	13.8	66	9.9	64	10.9	64	8.4	63	7.6
62	21.9	64	12.6	61	16.2	61	12.5	60	10.7
58	54.4	62	17	58	27.7	58	19.4	56	21.1
55	162.8	60	24.2	55	60.2	55	38.1	52	53.6
SOC=0.5		SOC=0.4		SOC=0.3		SOC=0.2		SOC=0.1	
P(W)	T(s)	P(W)	T(s)	P(W)	T(s)	P(W)	T(s)	P(W)	T(s)
64	4.2	60	4.6	55	6.2	52	4.5	48	1.5

62	5.1	58	6.1	53	8.9	48	8.9	45	1.8
58	8.6	55	9.4	48	22.4	45	16.4	42	3
54	16.7	50	25.5	42	72.4	42	23.9	38	5.9
50	42.7	45	73.8	37	150.9	37	47.8	33	13.2

Combining Tables 2 and 3, it can be seen that the constant power test method can achieve a reliable prediction for the duration (T=60s) within the duration. As the power of the battery increases, the discharge time decreases. Similarly, as the power to the battery decreases, the discharge time increases. The SOP fitting data at different durations are shown in Tab. 4.

Table 5. The SOP fitting data at different durations

SOC	Uoc	SOP(T=5s)	Idis(T=5s)	SOP(T=10s)	Idis(T=10s)	SOP(T=30s)	Idis(T=30s)	SOP(T=60s)	Idis(T=60s)
1	4.1716	74.3884	17.8321	67.7042	16.22979	60.5907	14.52457	58.2275	13.95807
0.9	4.0836	73.6392	18.03291	65.8979	16.13721	58.9411	14.43361	55.6954	13.6388
0.8	4.0317	71.9303	17.84118	64.7349	16.05648	57.6298	14.29417	55.0129	13.64509
0.7	3.9268	68.1853	17.36409	62.66	15.95701	55.8243	14.21623	54.2306	13.81038
0.6	3.8376	66.9205	17.43811	60.5565	15.77978	54.3649	14.16638	51.5334	13.42855
0.5	3.7482	62.9205	16.78686	56.6768	15.12107	51.4443	13.72507	48.5006	12.9397
0.4	3.665	59.3887	16.20428	52.372	14.28977	49.2767	13.44521	46.1201	12.58393
0.3	3.5866	56.1034	15.6425	48.581	13.54514	46.2767	12.90267	43.0229	11.99546
0.2	3.4789	51.3983	14.7743	47.5081	13.65607	40.7296	11.70761	34.6636	9.963954
0.1	3.3497	39.1388	11.68427	35.1802	10.50249	21.5259	6.426217	1.5014	0.448219

Where *Uoc* denotes the voltage parameter obtained by HPPC, Idis denotes the relationship between power and voltage at the current SOC. The Idis parameter reveals that the battery (with a measured capacity of 4.4Ah) has a maximum peak discharge current of 4C during the duration. In the first 30% SOC discharge, the peak power of the battery does not show large fluctuations with the decrease of SOC. Furthermore, by analyzing the variation of Idis, the power variation was largely related to the peak current, and when the Idis showed large fluctuations compared to the previous stage, the peak power output also showed drastic changes. Therefore, it is necessary to analyze the joint voltage and current limitation of the battery.

Combined with the above, it is difficult for the battery to provide a higher current to meet the power output when it is at 10% SOC. The power output at this time changes dramatically compared to the previous. And when the battery is in a longer period of peak power discharge, the power is difficult to verify the analysis. Therefore, the estimated power and error curve of the battery before 80% SOC discharge is shown in Fig. 14.

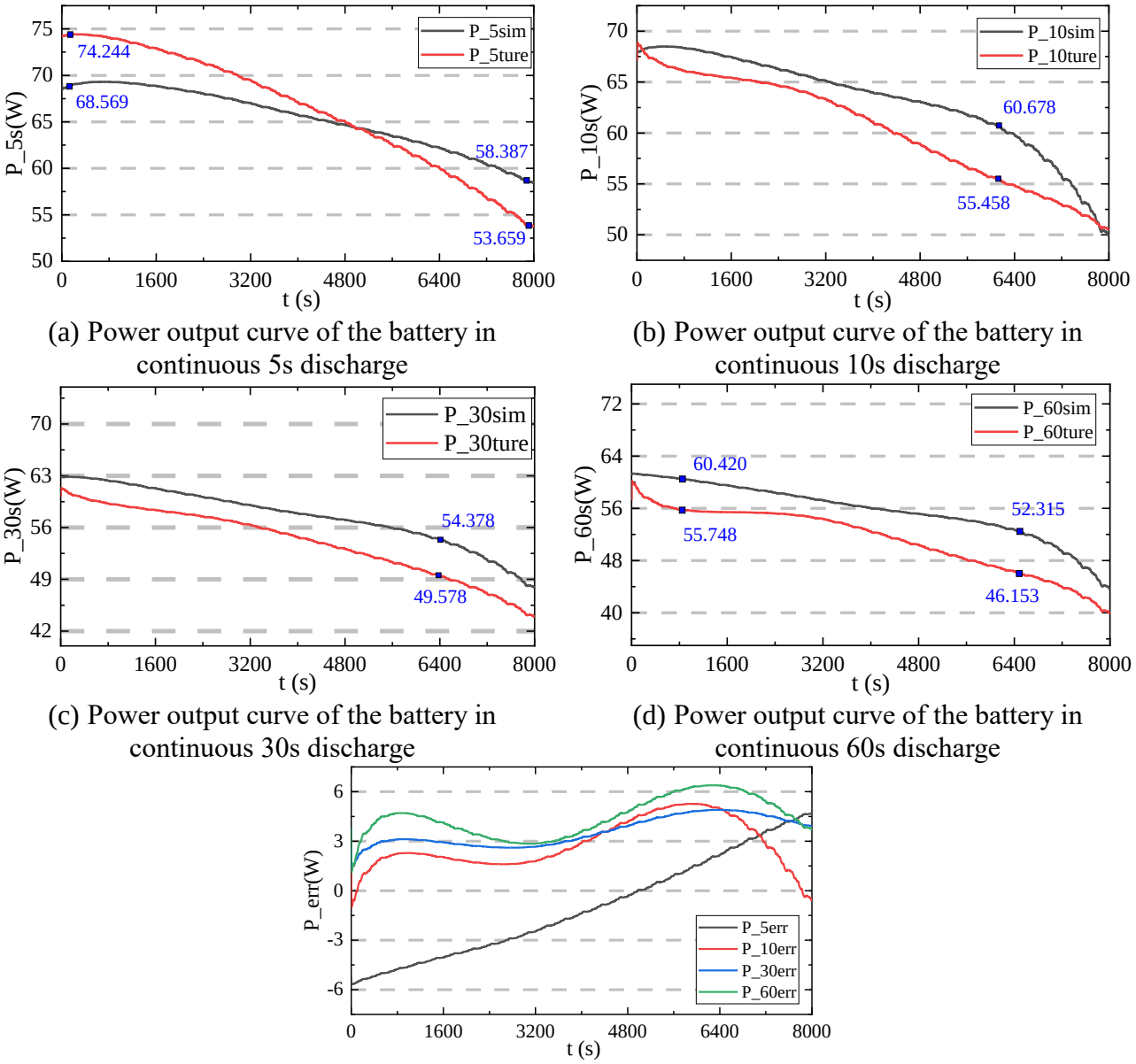

(a) Power output curve of the battery in continuous 5s discharge

(b) Power output curve of the battery in continuous 10s discharge

(c) Power output curve of the battery in continuous 30s discharge

(d) Power output curve of the battery in continuous 60s discharge

(e) Power output curves of batteries discharged at different durations

Figure 14. The estimated power and error curve of the battery before 80% SOC discharge

Where, *ture* represents the battery power output obtained by curve fitting analysis through the data in Table 4; *sim* represents the battery power output coupled with the power output of the battery using the fusion model analysis, and *err* represents the difference between the simulated power and the

actual power. From the Fig. (a), it can be seen that the simulated power in a short period of continuous discharge is an approximately straight line, which is due to the current limitation taking a larger proportion in the algorithm and suppressing the correction effect of other limitations; from the figures (b), (c) and (d), it can be seen that the correction effect of the fusion model is stronger in a longer period of discharge. In addition, it can be found from Fig. (e) that the estimation accuracy of the fusion model is high, with an error of less than 6W.

Therefore, the experiments show that the algorithm has a voltage error lower than 0.08V and an online power calculation error lower than 6W under BBDST conditions. Compared with many other models and algorithms, this method further optimizes the accuracy of the results and shortens the gap between theory and reality. Lai, Xin proposed a fractional-order model-based SOP estimation scheme to achieve reliable estimation for dynamic conditions by segmentation analysis of different SOC stages[30]. But in this paper, the SOP estimation is based on the fusion model of voltage, current and charge state, combined with temperature to realize online tracking and approximately ensure the real-time condition of the battery. Liu et al. used the capacity-temperature and resistance-temperature relationships from experimental data to more accurately predict the battery capacity and resistance over the entire temperature range, and used a multi-constraint algorithm to accomplish a reliable prediction of SOP[31]. Through the comparison between them, it is not difficult to find that the SOP error rate decreases by about 0.09%. Wei, Chun et al. deduced a battery SOP estimation algorithm considering both battery voltage and current constraints based on the circuit model of the identified parameters[37]. At the same time, the method has low complexity and numerical stability. Similiarly, in this paper, it focused on the online tracking model, and the parameters change with time. After all, the battery work is a dynamic process. As a result, the new method proposed in this paper can further approach the reality.

4. CONCLUSIONS

As an important indicator affecting the power effect of the battery, the accuracy of the lithium-ion battery power state affects the reliability and safety of battery use. A power state online tracking estimation method under the constraint of a fusion model for powered lithium-ion batteries considering temperature effects is proposed in this study. Firstly, the method achieves an effective analysis against the battery dynamic data through an improved adaptive forgetting factor recursive least-squares method with deviation compensation, avoiding the time-consuming pre-experiment and the voltage estimation error is less than 0.08 V. Secondly, the capacity of the battery is corrected by introducing the capacity change curve under the temperature environment change, and the effective estimation of SOC is achieved based on the online parameters. Finally, the prediction of power output test for different durations is achieved by constructing a fusion model with voltage, current, and charge state as the influencing factors. The experimental results show that the method can achieve a reliable prediction of the power state with an error of less than 6W.

ACKNOWLEDGMENTS
The work was supported by the National Natural Science Foundation of China (No. 61801407).

References

1. F. Gu, J. F. Guo, X. Yao, P. A. Summers, S. D. Widijatmoko and P. Hall, *J. Cleaner Prod.*, 161 (2017) 765.
2. A. Masias, J. Marcicki and W.A. Paxton, *Acs Energy Lett.*, 6 (2021) 621.
3. T. Xu, Z. Peng and L. Wu, *Energy*, 218 (2021) 77.
4. S. Sarvaiya, S. Ganesh and B. Xu, *Energy*, 228 (2021) 120064.
5. D. Zheng, H. M. Wang, J. J. An, J. Chen, H. H. Pan and L. Chen, *IEEE Access*, 6 (2018) 13170.
6. Z. Yun and W. Qin, *IEEE Access*, 8 (2020) 55447.
7. T. H. Wu and C. S. Moo, *Energy*, 10 (2017) 12.
8. X. H. Wang, W. H. Fan, S. X. Li, X. J. Li and L. Z. Wang, *Appl. Sci.-Basel*, 10 (2020) 19.
9. F. Xie, S. L. Wang, Y. X. Xie, C. Fernandezb, X. X. Li and C. Y. Zou, *Int. J. Electrochem Sci.*, 15 (2020) 7935.
10. H. X. Tian, P. L. Qin, K. Li and Z. Zhao, *J. Cleaner Prod.*, 261 (2020) 10.
11. X. Bian, L. Liu and J. Yan, *Energy*, 177 (2019) 57.
12. M. Zhao, T. Sun and Q. Feng, *Sci. Total Environ.*, 784 (2021) 11.
13. H. Dong, Q. Gong and M. Zhu, *Int. J. Electr Power Energy Syst.*, 130 (2021) 231.
14. J. T. He, Z. B. Wei, X. L. Bian and F. J. Yan, *IEEE Trans. Transp. Electrif.*, 6 (2020) 417.
15. J. Chen, X. Zhang, C. Li, X. Y. Zhang, Y. J. Ren, J. J. He and J. L. Chen, *Int. J. Photoenergy*, 2020 (2020) 2478.
16. H. Y. Xiong, H. Liu, R. H. Zhang, L. M. Yu, Z. J. Zong and M. H. Zhang, *Int. J. Hydrogen Energy*, 44 (2019) 29733.
17. J. Mao, D. Hong, R. W. Ren and X. Y. Li, *J. Coastal Res.*, 103 (2020) 1006.
18. Y. J. Zhang, Y. J. Huang, H. B. Chen, X. X. Na, Z. Chen and Y. G. Liu, *Energy*, 228 (2021) 12.
19. S. Ansah, H. Hyun, N. Shin, J. S. Lee, J. Lim and H. H. Cho, *Comput. Mater. Sci.*, 196 (2021) 1105.
20. Z. Chen, H. Q. Zhao, X. Shu, Y. J. Zhang, J. W. Shen and Y. G. Liu, *Energy*, 228 (2021) 120636.
21. N. Chen, P. Zhang, J. Y. Dai and W. H. Gui, *IEEE Access*, 8 (2020) 26872.
22. Y. Ma, X. Li, G. Y. Li, Y. F. Hu and Q. W. Bai, *IEEE Access*, 7 (2019) 156136.
23. J. F. Li, D. F. Wang and M. Pecht, *J. Power Sources*, 436 (2019) 233.
24. Q. Zhang, D. F. Wang, B. W. Yang, X. Cui and X. Li, *Electrochim. Acta*., 343 (2020) 136094.
25. L. J. Zhang, H. Peng, Z. S. Ning, Z. Q. Mu and C. Y. Sun, *Appl. Sci.-Basel*, 7 (2017) 10.
26. L. S. Liu, X. N. Feng, C. Rahe, W. H. Li, L. U. Lu, X. M. He, D. U. Sauer and M. G. Ouyang, *J. Energy Chem.*, 61 (2021) 269.
27. W. Xie, L. Y. Ma, S. Zhang, D. X. Jiao and J. C. Ma, *Electronics*, 9 (2020) 10.
28. X. T. Liu, Y. He, G. J. Zeng, J. F. Zhang and X. X. Zheng, *Energy Technol.*, 6 (2018) 1352.
29. P. Lin, P. Jin, J. C. Hong and Z. P. Wang, *Energy Rep.*, 6 (2021) 2299.
30. X. Lai, L. He, S. Y. Wang, L. Zhou, Y. F. Zhang, T. Sun and Y. J. Zheng, *J. Cleaner Prod.*, 255 (2020) 120203.
31. X. T. Liu, Y. He, G. J. Zeng, J. F. Zhang and X. X. Zheng, *Energy Technol.*, 6 (2018) 1352.
32. S. Xiang, G. D. Hu, R. S. Huang, F. Guo and P. K. Zhou, *Energies*, 11 (2018) 2.
33. Y. J. Wang, J. Q. Tian, Z. D. Sun, L. Wang, R. L. Xu, M. C. Li and Z. H. Chen, *Renewable Sustainable Energy Rev.*, 131 (2020) 110015.
34. W. X. Chen, C. Xu, M. L. Chen, K. Jiang and K. L. Wang, *J. Energy Storage*, 36 (2021) 102387.
35. T. Zhang, N. Y. Guo, X. X. Sun, J. Fan, N. F. Yang, J. J. Song and Y. Zou, *Sustainability*, 13 (2021) 9.
36. X. Lei, X. Zhao, G. P. Wang and W. Y. Liu, *Energies*, 12 (2019) 19.

37. C. Wei, M. Benosman and T. Kim, *Int. J. of Control Autom. Syst.*, 17 (2019) 2906.
38. M. J. Esfandyari, M. R. H. Yazdi, V. Esfahanian, M. Masih-Tehrani, H. Nehzati and O. Shekoofa, *J. Energy Storge*, 24 (2019) 100758